

Pick-up and photodissociation of hydrogen halides in floppy neon clusters

Petr Slavíček, Pavel Jungwirth *

*J. Heyrovský Institute of Physical Chemistry,
Academy of Sciences of the Czech Republic and Center
for Complex Molecular Systems and Biomolecules,
Dolejškova 3, 18223 Prague 8, Czech Republic*

Marius Lewerenz

*LADIR/Spectrochimie Moléculaire, UMR 7075, Bât F74, Bte 49,
Université Pierre et Marie Curie, F-75252 Paris Cedex 05, France*

N. Hendrik Nahler, Michal Fárník, and Udo Buck

*Max-Planck-Institut für Strömungsforschung,
Bunsenstrasse 10, 37073 Göttingen, Germany*

(Dated: June 20, 2003)

* Author to whom correspondence should be addressed.
Electronic mail: pavel.jungwirth@jh-inst.cas.cz

Abstract

Neon clusters with an average sizes in the range from $\langle n \rangle = 100$ to 1600 atoms are generated in an adiabatic expansion and are doped with a single HBr or HCl molecule in a pick-up process. The hydrogen halide molecule is photodissociated by a UV laser and the outgoing H fragment is ionized by resonance enhanced multi-photon ionization (REMPI) in a (2+1) excitation scheme at a wavelength of 243 nm. The H ions are extracted in a Wiley-McLaren time-of-flight mass spectrometer operating in the low-field mode to be sensitive to low velocities. The measured kinetic energy distribution are compared with quasi-classical molecular dynamics simulations, which allow for a detailed analysis of the underlying processes. Simultaneously, the neon cluster phase behavior, the pick-up procedure, and the photodissociation dynamics are investigated theoretically. The phase behavior is studied by means of the Instantaneous Normal Modes approach with a newly introduced projection technique, which allows us to disentangle the phases of the different cluster shells. For the cluster sizes investigated, the cluster core is basically solid or semi-liquid, while the outer shell is always liquid. Correspondingly, during the semi-classical pick-up simulation most of the HBr dopants stay in the surface of the cluster. Finally, the photodissociation simulation is performed starting either from the quantum mechanical ground state at $T = 0$ K or from a distribution at $T = 10$ K. It is demonstrated that the inclusion of the temperature effects is necessary to reproduce the experimental data and, therefore, plays a crucial role in the interpretation of the floppy neon clusters.

I. INTRODUCTION

Photodissociation of small molecules in different cluster environments has attracted a considerable interest in recent years. Special efforts were directed towards the hydrogen halide molecules interacting with different rare gas clusters. For many of these systems, the interaction potentials are well known. In addition, the calculation of the coupling in the manifold of the electronically excited states, which leads to the two spin-orbit states in the dissociation limit, is very demanding. For many years the field was dominated by an increasing number of theoretical contributions applying various theoretical approaches.¹⁻¹⁶ Since a couple of years also experimental data for the laser photolysis of this class of systems became accessible¹⁷⁻²¹ and the first direct comparison of measured and calculated quantities was carried out.⁹ The measured quantity is the kinetic energy of the outgoing H atoms which gives direct information on the cage exit and caging probability, corresponding to fast or slow values of the velocity. Experimentally, the molecules are placed on the surface by applying the pick-up technique, while the embedded site is produced in the co-expansion with the rare gas. One of the most intriguing results was the strong dependence of these data on the initial site (interior or surface) and on the specific surface state of the molecule. In addition, the embedded case was found to be strongly size-dependent, while the surface case was not. An interesting phenomenon was observed for the surface case by analyzing the dependence on the host cluster mass.^{18,19} The kinetic energy distributions originating from HBr (and also from HI) molecules resemble each other for the three heavier rare gases Ar_n, Kr_n, and Xe_n but differ from those measured for Ne_n clusters. There is, in addition, quite a similarity of the distributions of HBr-Ne_n with the embedded case of HBr-Ar_n (see Fig. 5 and Fig. 9 of Ref. 19). Apparently, different mechanisms govern the photodissociation of neon clusters and of the heavier rare gas clusters. The obvious and most plausible explanation for this behavior is that HBr and HI penetrate inside the neon clusters during the pick-up process so that surface states are not generated. Accompanying, preliminary calculations of the photodissociation dynamics showed indeed that the measurements are in much better agreement with the calculated embedded case than with the surface one.

The reason for this behavior might be that neon clusters in the size range investigated in these experiments, $\langle n \rangle \leq 150$, are liquid-like after the capture of an HX molecule. Such a process has recently been suggested in the interpretation of Xe doped Ne_n clusters.²²

By measuring the fluorescence excitation spectra of these clusters, only bulk states were observed up to cluster sizes of $\langle n \rangle = 200$. From $\langle n \rangle = 300$ onwards, also surface sites appeared in the spectra. The authors interpreted their results as a sort of phase transition from liquid-like to solid-like behavior. Such a transition should occur at a well defined size, if the melting temperature depends strongly on the cluster size.^{23,24}

If such an interpretation is correct, we should see similar effects in the photodissociation of HBr on Ne_n clusters where the cage exit probability can be used as probe of the state of the cluster matter. When the cluster becomes solid-like, the dopant stays on the surface and the cage exit probability increases. To resolve this problem, we carried out a series of new experiments both for HBr- Ne_n in the size range of $\langle n \rangle = 100$ to 1600 and, for comparison, also for HCl- Ne_n in the range of $\langle n \rangle = 100$ to 800. For that purpose a new source was constructed which allowed us to produce the large neon clusters by lowering the nozzle temperature to 60 K which was not possible with the source used in the previous experiments.

To rationalize the experimental results we have employed molecular dynamics simulation methods. It is imperative to describe correctly the initial state of the cluster under realistic experimental conditions. This means that we have to take into account the quantum zero point delocalization. This applies in particular to the librational motion of the HX molecule. For HX- Ne_n clusters the zero point motion and the anharmonicity can play a major role also for the cage modes. It is, in addition, important to account for temperature effects in these clusters. Neon clusters are expected to exhibit noticeable quantum effects. Therefore, a purely classical description is not suitable and we use semi-classical molecular dynamics simulations based on the Ehrenfest theorem²⁵ and the self consistent construction of quantum effective potentials to estimate the outcome of the pick-up process under experimental conditions. This method (see Sec. III B for details) is computationally very efficient and very well suited to systems with a priori unknown temperatures and size dependent properties. Subsequently, we apply molecular dynamics within the Wigner trajectories framework to calculate measurable quantities of the photodissociation experiment. At the same time, we investigate the neon cluster phase behavior at experimental temperatures as a function of cluster size.

The experimental results exhibit, surprisingly, no increase of the cage exit probability which would have been a manifestation of a solid-like surface state. The analysis showed

that the outer surface shells stay liquid also for the larger clusters and thus hinder the H atom dissociation fragments to leave the cluster in an appreciable number. The general applicability of these results will be discussed and compared with experimental results from other sources.²²

II. EXPERIMENT

The Ne clusters with an average size in the range from 100 to 1600, generated in our molecular beam apparatus, are doped with a single HBr or HCl molecule in a pick-up process. The hydrogen halide molecule is photodissociated by an UV laser pulse (HBr: 243 nm, HCl: 193 nm) and the outgoing H fragment is ionized by resonance enhanced multi-photon ionization (REMPI) in a (2+1) excitation scheme within the wavelength of 243 nm. The H ions are extracted in a Wiley-McLaren time-of-flight mass spectrometer (WM-TOFMS) operating in the so-called low-field mode where it is possible to transform the measured time-of-flight into a kinetic energy distribution of the H fragments. The experimental details with several improvements have been described elsewhere.^{8,17,26-28}

In contrast to former measurements¹⁸ with Ne clusters we increased the Ne cluster size with the help of a new cluster source shown in Fig. 1. Following the relation from Hagena²⁹ the average cluster size $\langle n \rangle$ is most effectively increased by decreasing the nozzle temperature T ($\langle n \rangle \propto T^{-2.2875}$ and $\langle n \rangle \propto p$). An increase of the expansion pressure p is limited by the capabilities of the vacuum pumps. Using a liquid nitrogen cooled conical nozzle (diameter: 47 μm , opening angle: 30°) at a minimal temperature $T_{min}(old) = 107$ K and an expansion pressure of 8.5 bar the maximum average Ne cluster size in the former experiments was limited to $\langle n \rangle = 143$. To achieve a lower nozzle temperature compared to the previous measurements, a two stage high-pressure helium compressor (LEYBOLD RGD 1245 + RW 4000EU) was employed. The expansion nozzle surrounded with a shielded electric heating coil is mounted in a copper block for cooling. The block is connected with a solid Cu-bar and flexible Cu-cables to the second stage of the cryostat. The nozzle is mounted in a Cu-shielding connected to the first stage of the cryostat to prevent the thermal radiation heating of the source. The gas inlet is realized with the standard 6 mm stainless-steel tubing and bellows. The entire nozzle assembly is centered in the shielding tube by circular teflon holders. The flexible Cu-cable connections to the cryostat allows for the nozzle position

adjustment with the fixed cryostat. This design minimized the nozzle heating and allowed us to achieve a minimal nozzle temperature of $T_{min}(new) = 55$ K. Depending on the nozzle geometry and the expansion pressure, with this source a Ne cluster size range from 100 to 1800 can be covered. The actual beam data used in the present experiments are given in Table I.

After the photodissociation of the hydrogen halide molecule the H atom can leave the cluster environment without any interaction with the cluster cage. In this case, which is rarely occurring for Ne cluster environments, the H atom behaves like one from the photodissociation of a free molecule. There are two highest possible energies of the H atom whether the halogen partner fragment populates the ground or excited spin-orbit state. Depending on the position of the molecule in the cluster environment and the direction where the H atom is pointing to, the fragment undergoes several collisions with the cluster cage which leads to a *delayed exit*. The amount of H atoms which lose all their kinetic energy in cage collisions is clearly not negligible and displays *perfect caging*. The details about the transformation of our measured time-of-flight spectra of the H fragments into kinetic energy distributions are described elsewhere.^{8,19,27}

III. THEORETICAL METHODS

A. System and potentials

We have investigated the photodissociation of HBr attached to large neon clusters with three and four icosahedral layers. In the classical simulations at $T = 0$ the three-layer cluster was represented by the icosahedral Ne_{147} cluster with one neon atom replaced by the HBr dopant. We have placed the dopant either into a substitutional position on the surface or into the central position (HBr embedded inside a neon cluster). The four-layer cluster has been represented by an icosahedral Ne_{309} cluster. For the simulation of photodissociation on clusters with finite temperature the adopted cluster sizes are slightly smaller than the closed layer structures. For the three-layer system the average cluster size was around 130 neon atoms (with a distribution which is given by the pick-up simulation procedure), while for the four-layer system the average size was around 290 neon atoms.

We used three sets of potentials. The first one was the potential energy surface for

the ground state of the HBr-Ne_n system, the second one was the potential for the excited state, and the third one was an effective ground state potential in which HBr is represented by a single pseudo-atom, which is used in the pick-up simulations. We constructed the ground state potential energy surfaces of the HBr-Ne_n clusters as a sum of two-body Ne-Ne interactions³⁰ and a three body potential for the HBr-Ne interaction.¹⁰ The bonding interaction between hydrogen and bromine is approximated by a harmonic potential.³¹

The above described HBr-Ne_n ground state potential was used for the calculation of the initial librational and vibrational wavefunctions (for simulations at $T = 0$). The simulation of the pick-up process is, however, very long (≈ 50 ns). The computational cost would become prohibitive, since rigorously the delocalization of strongly quantum HBr has to be taken into account, which involves the computation of the librational wavefunction by diagonalization whenever the energy is calculated. We have, therefore, constructed effective HBr-Ne potentials by averaging the HBr orientations over all possible angles. Here, we modeled the bound HBr molecule in neon as a free rotor. This turns out to be a reasonable approximation for such a weakly bound system. This effective potential has been fitted to a Lennard-Jones form:

$$V_{LJ} = 4\epsilon \left\{ \left(\frac{\sigma}{r} \right)^{12} - \left(\frac{\sigma}{r} \right)^6 \right\} \quad (1)$$

with $\sigma = 3.45$ Å and $\epsilon = 34.2$ cm⁻¹. Note also that our assumption of HBr behaving as a free rotor is perfectly adequate for HBr embedded in the neon cluster, while it leads to a slight underestimation of the binding energy on the surface.⁹

The potential in the excited state has been modeled as a sum of H-Br interaction in the ¹Π₁ or ³Π₀ state^{12,32} and pairwise Br-Ne, Ne-Ne and Ne-H interactions. The ¹Π₁ state correlates with the ground state H+Br asymptote. Note that at the excitation wavelength of 243 nm mainly the H+Br state is populated in the gas phase with a branching fraction of 0.83 (see Ref. 27). Nevertheless, we also run photodissociation simulations on the ³Π₀ state surface corresponding to the H+Br* spin-orbit excited asymptote. These two channels are not coupled in our simulations. We have omitted the contribution from the ³Π₁ state, which correlates also with the ground state asymptote, therefore, the dynamics is almost identical to that on the ¹Π₁ state. For computational simplicity the Br-Ne interaction is assumed to be isotropic and is modeled by a Morse potential.³³ The adopted neon pair potential is the same as that for the ground state.³⁰ The Ne-H potential in the repulsive region up to

approximately 2 eV was not readily available. Therefore, we calculated 25 *ab initio* points for Ne-H distances ranging from 1.1 Å to 4.0 Å at the CCSD(T)/aug-cc-pVQZ level, which were subsequently fitted to the following functional form:

$$V_{Ne..H}(r) = 1.39517 \exp(-1.03853r - 0.11095r^2), \quad (2)$$

where all parameters are in atomic units. This parametrization provides a perfect fit to the *ab initio* values in the repulsive region.

B. Construction of effective quantum potentials

Neon clusters exhibit noticeable quantum effects, which represent a challenge for dynamical simulations. These quantum effects influence the binding energy per particle (the ground state binding energy is only about 60% of the well depth) and the mean particle distances. Presumably, they will have also an important effect on the dopant embedding dynamics, the dopant mobility inside the cluster, and the number of neon atoms evaporating after the impact of the dopant.

A full quantum dynamical simulation of dynamic properties of neon clusters is impossible with present computational techniques. We have thus resorted to an approximate technique which attempts to include the above mentioned main quantum effects via the construction of effective potentials V_q . Basically, each particle is represented by a single particle wavefunction and the Ehrenfest theorem is applied. Particle positions evolve according to classical dynamics on the effective potential. This approach is appropriate if the single particle wave function is sufficiently compact, i.e. quantum effects are not overwhelming.³⁴

Similar ideas have been used with good success even for quantum solids like hydrogen.³⁵ In the latter case a gaussian shape was assumed for the single particle wave functions, the spread of which was adjusted by comparison of simulation results with known bulk properties. Effective quantum potentials are also among the results of the Feynman-Hibbs treatment³⁶ which has been applied to pure neon clusters in the past.³⁷ While it is possible to construct effective quantum potentials for bulk systems by fitting particle binding energies, bulk densities, and pair correlation functions, our strategy for the construction of the effective quantum potential for clusters avoids the use of empirical information. We use a self consistent iterative procedure, which has been applied previously with surprising success

to pure and doped helium clusters.³⁸ This method is particularly suitable for clusters where empirical density and pair correlation information are not available. Conceptually, each particle is replaced by a probability distribution $\phi^2(r)$ (note that the ground state wavefunction is real), centered around its classical position, and assumed to have a spherical symmetry. Starting from the original pair potential $V_{cl}(R) = V_{q,0}(R)$, $R = |\mathbf{R}|$ representing the interatomic distance, a delta distribution $\phi_0^2(r)$, and known masses the construction is based on the following sequence of calculations, which is repeated until the n -th order quantum effective potential $V_{q,n}$ and all distributions have reached self consistency:

1. Construction of the pair correlation function $P_n(R)$ between classical particle positions from a classical molecular dynamics simulation at temperature T with the current potential $V_{q,n}(R)$.
2. Convolution of the pair correlation function with the current single particle distribution $\phi_n^2(s)$ according to

$$P_{q;n}(|\mathbf{R}|) = \int P_n(|\mathbf{R}|)\phi_n^2(|\mathbf{R} - \mathbf{R}'|)d\mathbf{R}'. \quad (3)$$

3. Construction of the radial potential $V_{rad;n}(r)$ experienced by each particle in the 'cage' formed by the other particles by integration over the current pair potential and the particle distribution following

$$V_{rad;n}(|\mathbf{r}|) = \int V_{cl}(|\mathbf{r} - \mathbf{R}|)P_{q;n}(|\mathbf{R}|)d\mathbf{R}. \quad (4)$$

4. Solution of the radial Schrödinger equation in the radial potential $V_{rad;n}(r)$ in order to find $\phi_{n+1}(r)$ for each particle in the mean field of the others.
5. Construction of the next generation effective pair potential $V_{q;n+1}(R)$ by the convolution

$$V_{q;n+1}(R) = \int \int V_{cl}(|\mathbf{R} + \mathbf{r} - \mathbf{r}'|)\phi_{n+1}^2(|\mathbf{r}|)\phi_{n+1}^2(|\mathbf{r}'|)d\mathbf{r}d\mathbf{r}'. \quad (5)$$

The algorithm was described for the construction of an effective potential for the Ne-Ne interaction. The effective potential for the Ne-dopant interaction can be constructed in a similar fashion with two distinct radial distributions. All radial and pair potentials are computed on a grid and spline interpolated for the molecular dynamics simulations and for the

solution of the Schrödinger equation. The number of iterations required to reach self consistency is modest. Fig. 2 shows the convergence of the effective potential. The figure depicts the classical potential, the first iteration and the 10th iteration which is already converged. Actually, only 4 iterations are required for a fully converged effective quantum potential in this case. The 'broadening' of each particle described by ϕ_n tends to partially fill the potential well and to leads to a shift to larger mean particle distances and thereby accounts semi-quantitatively for the quantum zero point effects. The change in the effective well depth in fact reproduces surprisingly well the amount of zero point energy in the system and the change in mean particle distances accounts very well for the change of the bulk density upon inclusion of quantum effects.³⁸ The resulting potentials are clearly temperature dependent and could be reconstructed periodically during a non equilibrium impact simulation. This would make sense if we were interested in the first stage of the pick-up process, i.e., in the collision. We address, however, the question what is the final dopant distribution, therefore, this recalculation of the effective quantum potential is not required. All the distributions obtained by the temperature dependent effective potentials are distributions of vibrationally averaged structures. Note also that (unlike, e.g., the Feynman-Hibbs potential) our effective quantum potential is size dependent. This corresponds to the fact that smaller systems tend to exhibit a more pronounced quantum character. Thus, this approach is well suited for the study of large clusters with moderate quantum effects.

C. Pick-up simulations

Mixed molecular clusters can be prepared by two different techniques: (i) by co-expansion in which case a mixture of the dopant with rare gas is expanded into the vacuum, or (ii) by a pick-up procedure in which pure rare gas clusters prepared by a supersonic expansion travel across a chamber with the dopant. For solid systems one is thus able to create doped clusters where the dopant occupies different positions in or on the cluster according to the way of preparation. However, for ergodic systems (e.g., for liquids) the final dopant sites are simply given by the equilibrium thermodynamic distributions and they are thus independent of the cluster preparation technique. Molecular dynamics simulation can help in answering the question what is the distribution of positions under experimental conditions corresponding to the pick-up process.³⁹

The outcome of the molecular dynamics simulation is strongly dependent on the composition, cluster temperature, cluster beam velocity, and buffer gas temperature. The specific question in the present context is the final dopant position for HBr picked up by neon clusters with three and four icosahedral layers. Note at this point that molecular dynamics is the appropriate simulation tool for answering this question. It is essential to perform non-equilibrium dynamical (and not thermodynamical) simulations because (i) we do not know in advance the final temperature of the system and (ii) for non-ergodic systems the final distribution can represent just a local minimum of the free energy surface of the system, i.e. a metastable state with high kinetic stability. Molecular dynamics simulations can thus provide important insight into the character of doped clusters formed under typical experimental conditions, and at the same time these simulations can serve for testing ground state potentials.

For the integration of Newton equations of motion we have employed a standard Verlet algorithm.⁴⁰ The time-step was set to 10 fs, which is a reasonable choice for this type of systems.³⁹ The initial cluster temperature was set to 10 K. Clusters were equilibrated for 10 ns and then allowed to collide with a dopant under a random angle and with a relative velocity distribution given by the buffer gas (containing the dopant) temperature $T = 300$ K and the velocity of the rare gas cluster beam. The cluster beam velocity is set to 450 ms^{-1} , which is the value measured in the experiments. The pick-up simulations typically cover a total time of 70 ns. Longer times were used in a small number of test simulation runs, but did not lead to any significant changes in the resulting distribution. All monitored quantities were recorded every 100 time steps. For each cluster size 200 trajectories have been collected.

We followed two quantities which indicate the final position of the dopant in or on the cluster. The first one is the distance of the dopant from the cluster center of mass (r_{com}), while the second quantity is the number of nearest neighbors of the dopant N_n . A nearest neighbor is defined as any solvent atom within a sphere of radius 4.3 Å around the dopant. The corresponding distribution functions $\rho(r_{com})$ and N_n have then been calculated.

Neon clusters at a temperature of $T = 10$ K are systems of moderate quantum character and this has to be taken into account. This is achieved using effective quantum potentials constructed by the procedure described in Sec. III B. Furthermore, we have substituted the three body HBr-Ne potential by an effective two body potential as described in the beginning

of Sec. III A.

We chose clusters with an almost complete outer shell as representatives of three or four layer clusters. In order to increase the isomerization rates and thus the convergence of the pick-up simulation we did not use closed shell clusters with high icosahedral symmetry. Test simulations of the pick-up process for closed shell clusters showed no significant difference, except for slower equilibration. We should stress that under experimental conditions a rather broad cluster size distribution is produced.⁴¹

D. Instantaneous normal mode analysis of cluster phase behavior

The Instantaneous Normal Modes (INM) analysis is a valuable tool for the description of the liquid state,^{42,43} especially for short time dynamics. Moreover, the density of states calculated by the INM method can help to distinguish between solid and liquid phases. Here we use INM as a tool for analyzing the phase behavior of neon clusters of different sizes and apply it separately to different neon layers.

We have constructed the Hessian matrix in a mass-weighted atomic cartesian coordinate basis $x_{n\mu}$ of N atoms, with $\mu=\{x, y, z\}$. For a given instantaneous position \mathbf{R} the Hessian matrix element reads:

$$D_{n\mu,n'\mu'}(\mathbf{R}) = \frac{\partial}{\partial \mathbf{x}_{n\mu}} \left(\frac{\partial V}{\partial \mathbf{x}_{n'\mu'}} \right)_{\mathbf{R}}, \quad (6)$$

where V is the interatomic potential. Diagonalization of the Hessian matrix provides $3N$ eigenvalues λ_i , which are related to harmonic frequencies by

$$\omega_i^2(\mathbf{R}) = \lambda_i(\mathbf{R}). \quad (7)$$

The elements of the $3N$ eigenvectors describe the contribution of each atom to the i -th mode. The essential output of the the INM procedure is the density of states. This is identical to the histogram of frequencies averaged over an ensemble of configurations obtained by molecular simulation techniques:

$$\rho(\omega) = \left\langle \sum_{i=1}^{3N-6} \delta(\omega - \omega_i) \right\rangle. \quad (8)$$

The six frequencies corresponding to rotational and translational motions of the whole cluster have been omitted from the histograms.

Due to the diagonalization at instantaneous configurations, imaginary frequencies (i.e., negative eigenvalues of the Hessian matrix) may occur. These frequencies reflect regions of negative curvature on the potential energy surface in the vicinity of saddle points and barriers. Imaginary frequencies are typical features of the liquid state, the fraction of imaginary modes being related to the self-diffusion constant of the system. For solids no imaginary frequencies are observed, and the entire spectrum is usually shifted towards higher frequencies. Previous work on several systems has shown that the INM density of states provides a sensitive probe of the liquid vs. solid state of a cluster.⁴⁴⁻⁴⁶

One of the advantages of the INM analysis is that we can perform projections of the density of states. The density of states spectrum can be decomposed, e.g., into molecular rotational and translational motions.⁴³ For molecular clusters it is interesting to explore the localization of the motion described by the Hessian eigenvectors at different frequencies. Even though the harmonic modes are inherently collective, certain motions can be attributed to a limited region of the system. This is the case for inhomogeneous systems, where the spectral characteristics can be quite different for different spatial parts. We define a projector P_{area} :

$$P_{area} = \sum_{n \in area} \sum_{\mu=x,y,z} c_{n\mu}^2, \quad (9)$$

where area can be, e.g., a certain cavity around the host molecule. The projected density of state is then given as:

$$\rho^{area}(\omega) = \left\langle \sum_{i=1}^{3N-6} P_{area} \delta(\omega - \omega_i) \right\rangle. \quad (10)$$

With the use of the above projection technique, we have addressed the question concerning the phase behavior of different cluster layers of neon clusters under experimental conditions. We have, therefore, calculated the density of states spectra projected on the first, second, third and fourth neon layer.

A critical issue is the sampling of instantaneous configurations for the INM analysis. Usually, classical molecular dynamics or Monte Carlo techniques are employed. Here we deal, however, with a moderately quantum system. Thus the Path Integral Monte Carlo

method would be an ideal choice⁴⁷ if we were not also interested in certain dynamical aspects of the process. We have chosen a simpler method based on classical molecular dynamics on effective quantum potentials, similarly to the simulations of the pick-up process.

E. Initial state sampling

In order to run quasi-classical molecular dynamics simulations of the photodissociation process we need a set of initial coordinates and momenta of the HX-Ne_n systems. Here we briefly describe the sampling of initial state at (i) $T = 0$ K, or (ii) at a finite temperature of $T = 10$ K.

For the sampling of the initial state at $T = 0$ we have adopted a similar approach as in our previous studies.^{9,10} We have started from optimal icosahedral structures of neon clusters with three or four layers (Ne₁₄₇ or Ne₃₀₉). These clusters have been chosen because of their high symmetry and stability (magic number clusters). Then we have replaced one of the neon atoms by an HBr dopant and we have optimized the structure. The process of structure optimization is performed simultaneously with the calculation of the vibrational wavefunction and is described in the next paragraph. The HBr dopant is placed either in the surface or in the center of the cluster. There is only a small number of distinct substitutional positions in the outer layer and a single well defined center of the cluster.

We have calculated the initial wavefunction in the following factorized form:

$$\Psi(\rho, q_1, q_2, \dots, q_{3n-6}, \Theta, \Phi) = \frac{\chi(\rho)}{\rho} \phi_1(q_1) \dots \phi_{3n-6}(q_{3n-6}) \phi_{lib}(\Theta, \Phi, \{q_i\}) \quad (11)$$

where q_i are the normal coordinates of the cage (i.e., heavy atoms) and ρ is the H-Br separation. The factor $1/\rho$ arises from the use of spherical coordinates. Cage modes are taken into account within the harmonic approximation which somewhat underestimates the quantum delocalization of neon. The librational part of the wavefunction is calculated by diagonalization of the hindered rotational motion of HBr in the basis of symmetry adapted spherical harmonics. The corresponding Hamiltonian is:

$$\hat{H} = \frac{\hat{j}^2}{2\mu_2 r^2} + V(\Theta, \Phi, \{q_i\}) \quad (12)$$

where μ is the reduced mass of the HBr molecule and $V(\Theta, \Phi, \{q_i\})$ is the full potential energy

surface of the system. The librational wavefunctions and eigenvalues depend parametrically on the cage coordinates. We took advantage of an adiabatic separation between the fast HX librational motion and the slow cage motions. The optimal cage structure has been found by optimizing the librational energy (i.e., the lowest eigenvalue of the librational Hamiltonian) with respect to the cage modes. For the optimal structure we have calculated the normal modes of the cage. Finally, we have carried out the Wigner transformation⁴⁸ to map the wavefunction onto the classical phase space.

A different approach is used for constructing initial states of the systems at a finite temperature. For that we have simply taken the final state sampled by the semi-classical molecular dynamics simulations (described in the section IIIB) of the pick-up process. In this way we sample the vibrationally averaged distribution of heavy particles at a given temperature. Using this treatment, we have, at least approximately, taken into account the anharmonicity of the Ne-Ne and Ne-HBr potentials. Also the temperature effect is included by this approach. For the cage structures obtained from the MD simulations, we have diagonalized the librational wavefunction. In this way, we go beyond the isotropic approximation for the HBr-Ne interaction.

F. Photodissociation dynamics

The initial vibrational state of the system is strongly quantum mechanical and in particular the angular motion of HBr has to be described properly. However, after the photoexcitation the system acquires more than 1 eV of excess energy and, therefore, the dynamics is then in a good approximation driven by the classical laws of motion. In our simulation we took advantage of this fact by running classical dynamics with positions and momenta sampled from a Wigner distribution.⁴⁸

Direct use of the Wigner distribution of initial conditions for molecular dynamics simulations corresponds to a vertical excitation. In the experiment, however, a fixed excitation wavelength is used. Therefore the condition

$$\hbar\omega = E_{Ne-HBr}^e - E_{Ne-HBr}^g \quad (13)$$

has to be fulfilled. Here, $\hbar\omega$ is the energy of the exciting photon, and E_{Ne-HBr}^g and E_{Ne-HBr}^e are the interaction energies between Ne and HBr in the ground and in the excited states.

In practice, we have conducted the energy filtering as follows. First, we have sampled the librational and cage motions (see previous subsection). Then, we have extended the HBr bond distance to a value which satisfies the above energy criterion. For the description of the HBr dynamics upon photoexcitation with a 243 nm laser pulse, we have adopted a two state model. The dynamics occurs primarily on two surfaces: $^1\Pi_1$ and $^1\Pi_0$ corresponding to the H+Br and H+Br* asymptotes. The $^3\Pi_1$ state which we did not take into account also correlates with the ground state asymptote. For the HI molecule, we have tested that the KEDs obtained from photodissociation on the $^1\Pi_1$ and the $^3\Pi_1$ states are practically identical.⁴⁹ This is because the hydrogen kinetic energy distribution is primarily governed by the available excess energy and not by the detailed shape of the repulsive potential. It has been shown,³² that non-adiabatic transitions do not play a role in the photodissociation dynamics at an excitation wavelength of 243 nm. Since the HBr molecule is promoted close to the crossing point of the $^1\Pi_1$ and $^1\Pi_0$ state, it is unlikely that the molecule would return to it during the dissociation process. As a result we expect that the branching ratio between the Br and Br* asymptotes in the cluster does not differ significantly from its value in the gas phase. We have, therefore, adopted a branching fraction of 0.83 for the H+Br asymptote.²⁷ The simulated experiment uses polarized laser beam, however due to a scattering from the cage the mixing of different states occurs.⁴⁹ Altogether 1000 Wigner trajectories have been sampled for the simulation at $T = 0\text{K}$ and several thousands of trajectories have been collected for simulations at $T = 10\text{K}$. The simulation time was 3 ps with a time step of 0.0241 fs.

IV. RESULTS

A. Experiment

The experimentally measured kinetic energy distributions of the hydrogen atoms originating from the photolysis of HBr and HCl molecules in Ne cluster environments are depicted in Fig. 3 and 4, respectively. The dependence of these kinetic energy distributions on the average Ne_n cluster size was measured. The size range covered in all these measurements corresponds to clusters from 100 Ne atoms (less than three closed icosahedral shells) up to 1600 Ne atoms (more than 8 shells). Figure 3 shows example distributions for three average

sizes $\langle n \rangle = 1600, 400$ and 200 , from top to bottom. The most pronounced feature in all three distributions is the peak rising at zero kinetic energy, corresponding to the *perfect caging* of H atoms. There is little evidence for *direct cage exit*, which is expected to appear at approximately 1.3 and 0.9 eV, corresponding to the H atoms leaving behind Br in the ground and excited spin-orbit states, respectively. Remarkably little size dependence is observed in the distributions, apart from the increasing error bars with decreasing cluster size, which are due to the lower absolute signals at smaller cluster sizes. This is also confirmed by the other measurements within and further below the depicted size region, which are not shown here. We note that close to the lower size limit the data taken in the old arrangement have better signal to noise ratios than the current ones.

The prevailing *perfect caging* indicates sinking of the HBr molecule into the cluster, which is only possible in locally melted or liquid clusters. Also the little difference between the distributions at various cluster sizes does not seem to support the phase transition from liquid to solid clusters suggested to occur for cluster sizes between 200 and 300 Ne atoms,²² which was expected to lead to a larger fraction of HBr molecules residing on the surface and thus contributing to more direct cage exit events.

Figure 4 shows the H atom kinetic energy distributions from photodissociation of HCl molecules on Ne clusters. From the covered average cluster size region between 100 and 800 Ne atoms, three example distributions are shown with $\langle n \rangle = 800, 200$, and 147 . Again the distributions are dominated by *perfect caging*. Also consistent with the above results for HBr is the absence of direct exit in the present distributions. At the top distribution for $\langle n \rangle = 800$, the *delayed exit* channel seems to increase in significance. This corresponds to hydrogen atoms, which do not undergo enough collisions to lose most of their kinetic energy on their way out, and leave the cluster with some part of the energy gained in the photodissociation process. This in turn might indicate an increasing fraction of HCl molecules, which do not sink deep enough into the larger Ne clusters. We note that for HCl, in contrast to HBr, neither the photodissociation of HCl-Ar_n clusters exhibits very pronounced cage exit probabilities.⁵⁰ Thus the HCl-Ne_n clusters do not show such a different behavior from the argon analogues as the HBr-Ne_n clusters do.

B. Pick-up simulations

The experimental results of the photodissociation of HX dopants on neon clusters of different sizes suggest a liquid character of the neon clusters. Indeed, the previous experience with the HBr-Ar_n system⁹ shows that a significant fraction of the fast hydrogen kinetic energy component is present for the surface HX-Rg_n clusters, while the comparison of the calculated kinetic energy distribution (KED) spectra of HBr-Ne_n at $T = 0$ K clusters with HBr in the center or on the surface of the neon cluster leads to the conclusion that the HBr dopant is penetrating the cluster (see part D of this section). This conclusion is, however, in contradiction with the size dependence of the experimental KED spectra of HBr-Ne_n and HCl-Ne_n clusters. From other experiments it was concluded from the existence of surface states that large neon clusters should be solid under experimental conditions.²² We have, therefore, directly addressed the question of the final position of the HBr dopant after the pick-up process, in order to clarify this seeming controversy.

For this purpose, we have explored the behavior of the clusters during the pick-up process for two representative cluster sizes. Neon clusters with the initial sizes around Ne₁₃₀ and Ne₃₀₀ have been selected to represent clusters with three and four layers. We deliberately did not use the perfect icosahedra (i.e., Ne₁₄₇ and Ne₃₀₉) in order to increase the isomerization rates. As was discussed before, neon clusters are moderately quantum systems. The quantum character of neon was taken into account by the use of effective quantum potentials describing both the Ne-Ne and the Ne-HBr interaction as was discussed above. The HBr molecule is represented as unified Lennard-Jones atom (see Sec. III).

Figure 5 displays the result of HBr pick-up on the neon cluster with 130 neon atoms. The simulation can be visualized in two ways. The upper part of Fig. 5 depicts the density of the dopant atom as function of the distance from the center of mass of the cluster. For comparison, also the density of neon atoms is added in the graph. The majority of the dopant atoms stays in the surface area of the cluster in the third shell. There is also a peak near the central position of the cluster. Note, however, that the depicted quantity is a density, which should be multiplied by a factor of $4\pi r^2$ to obtain the number of dopant atoms. Thus, only approximately 7 % of the dopants land in fully embedded positions. Most of the dopants stay deeply in the third shell, often on the border to the second shell. The Ne₁₃₀ cluster is apparently of a semi-liquid character after the impact of the dopant,

occasionally enabling the dopant to reach the center. However, the position in the surface is thermodynamically preferred. Another way to visualize the final solute distribution in the cluster is to display the number of neon atoms in the immediate neighborhood of the dopant (i.e. closer than 4.3 Å). The resulting distribution is displayed in the lower part of Fig. 5. Fully embedded dopants are those with the number of nearest neighbors larger than 15 (note that also some of the neon atoms from second solvation layers are occasionally counted). Most of the dopants are interacting with either 6 neon atoms or with approximately 10 neon atoms (which corresponds to the dopant position between the third and the second layer). There is no evidence for a smooth adsorption site of the HBr dopant on the neon clusters, in which case, one would expect the HBr molecule to directly interact with only approximately 3 neon atoms.

The situation for the Ne_{300} cluster is different. Neon clusters with four solvation layer are much stiffer than clusters with three layers. Moreover, quantum effects are less important for larger clusters since neon atoms are more confined. As a result, none of the HBr dopants penetrates into the fully embedded position (corresponding densities for dopant and neon atoms are depicted in the upper part of Fig. 6). Most of the HBr particles stay deeply solvated in the outer, fourth neon layer. There is also a small portion (6 %) of dopants in the smooth adsorption position. This amount is, however, too small to allow us to precisely decide whether it is only an artefact of the short duration of the pick-up simulation or whether the occupation of this position actually reflects the genuine thermodynamical distribution. The lower part of Figure 6 shows the number of nearest neighbors of the HBr dopant for the same system. We can observe the typical feature of the surface solvation with 6-10 solvent atoms closer than 4.3 Å. This result indicates that the cluster core is solid after the pick-up of the dopant and the part of the phase space with deeply embedded dopants is virtually not accessible under the experimental conditions.

C. Cluster phase behavior

One of the important issues addressed in our simulations is the character of the clusters studied. Are these clusters solid or liquid under the experimental conditions? If they are liquid, then the distribution that we observe in the pick-up and, consequently, in the photodissociation simulations should correspond to a statistical distribution at a given temper-

ature. If, however, the clusters are solid then both in the simulations and in the experiment we observe metastable states with a very long lifetime rather than an equilibrium thermodynamical distribution. This question can be resolved by means of the instantaneous normal modes (INM) density of states (DOS) spectrum. The typical INM DOS spectrum for a liquid differs significantly from that for a solid. The DOS spectrum of an atomic liquid has a right triangular pattern for the distribution of real frequencies corresponding to the translational motion of the atoms.⁴³ This shape is caused by a dominant presence of the slow, soft modes in liquids. Furthermore, a significant fraction of imaginary frequencies is present in liquids (imaginary modes are usually depicted for convenience on the negative part of the axis of the DOS spectra). Imaginary frequencies are not present in solid systems. Moreover, the right triangular shape of the positive part of the spectrum disappears as well. The spectrum for an atomic bulk solid shows other spectral features, corresponding to transverse and longitudinal phonon modes which give rise to peaks and singularities with a characteristic gap between zero and the onset of the first peak. In clusters the sharp features are replaced by broader peaks which represent the contributions from the different shells and, at lower frequencies, the surface contribution appears.⁵¹ But the gap at very low frequencies continues to be present as long as the cluster remains solid.⁵² As expected, for larger clusters the signal from the surface part decreases at the expense of the interior fraction.

We calculated the INM DOS spectra for clusters of approximately the same size as those in the pick-up simulations, i.e., with 130 or 300 neon atoms. We applied the projection technique described in the Sec. III. D to investigate the phase behavior of the neon atoms in different cluster layers. The upper panel of Fig. 7 depicts the INM DOS of the Ne_{130} cluster at 10 K. This temperature is the one determined from electron diffraction data of a supersonic neon cluster beam.⁵³ The DOS of the interior part of the cluster shows very few imaginary frequencies. However, their presence allows us to conclude that a cluster of this size is at the border line of the fully liquid cluster, close to the phase transition. Still, the core of the cluster is more a solid than liquid. Moving closer to the surface of the cluster, the character of the density of states changes. Now, it is a typical spectrum of a liquid with the right triangular shape in the real part of the spectrum and with a significant imaginary frequency contribution.

The INM DOS spectrum for the interior part of the Ne_{300} cluster as displayed in the lower panel of Fig. 7 exhibits features typical for a solid. The frequency distribution is

shifted towards higher values and no imaginary frequencies are observed. This is basically true for all the layers except for the outermost one, which is apparently liquid. It is interesting to compare these cluster DOS with those calculated or measured for a bulk phonon spectrum.^{54–56} The three arrows indicate the positions of the transverse and longitudinal peaks of solid neon. The frequency range is already covered by the two innermost shells, but the sharp peaks and edges of the well ordered solid are completely washed out. In addition, there are large intensity contribution at smaller frequencies which originate from the surface positions. Thus the transition to the bulk limit is rather slow in this cluster size regime.

We summarize that, at $T = 10$ K, the Ne_{130} clusters with three icosahedral layers have a semi-liquid core, while Ne_{300} clusters with four layers have a fully solid core. The outer shell is in both cases liquid and the dopant stays deep in this surface layer. For smaller clusters, the dopant is solvated in the surface on the average by more neon atoms than in large clusters. We do not find the suspected complete liquid to solid transition in this size range, but it might very well be the case that the melting of the cluster is a gradual process setting in at the surface.

D. Photodissociation dynamics at $T = 0$ and at finite temperature

In this section we compare our calculations of the kinetic energy distribution of the hydrogens leaving from the cluster with the corresponding measured spectra of HBr-Ne_n systems. Initial simulations were conducted at $T = 0$. Recall that here we assume the dopant and the cage to remain in its optimal positions, and the cage to be described by a harmonic wavefunction. While these approximations work well for argon clusters,¹⁰ the less bound and lighter neon clusters require more caution. The results of such simulations for HBr-Ne_{146} are shown in Fig. 8. We have calculated the KED either for the cluster with HBr in the surface substitutional position (upper panel of Fig. 8) or in the central position of the icosahedral cluster (lower panel of Fig. 8). For comparison, the experimental result of the photodissociation of the HBr-Ne_n cluster prepared by a pick-up process for the average size $\langle n \rangle = 143$ is added. All KED spectra, both the simulated and the experimental ones, are normalized the same way, and can thus be directly compared. It is immediately visible that the simulation for the interior case is in a better agreement with the experiment than that for the surface position. For the surface case the simulation predicts a far too low component

at zero energy and a too intense fast component of the outgoing hydrogen atom with about the same amplitude as the peak at zero energy. The fast component in the KED spectrum results from direct hydrogen atom reflection from the cluster surface. Once the hydrogen atom enters the cluster after the photodissociation, it is slowed down, since it undergoes many collisions before eventually escaping again. The fraction of the reflected hydrogen atoms is mainly determined by the HBr position in the surface and by the the distance between neon atoms. The further the HBr molecule is from the cluster center of mass and the closer the neon atoms are to each other, the larger is the amount of reflected hydrogens. The HBr molecule is slightly too large to perfectly fit into a substitutional position of the neon cluster. The cluster thus tends to expel the HBr dopant outside from the cluster even though the energetics favors slightly the HBr-Ne interaction over the Ne-Ne one. Comparison of the simulations of the surface versus the embedded case would suggest that during the pick-up process HBr does not stay on the surface of the cluster but penetrates deeper inside the cluster. The experiment, however shows very similar spectra for the clusters up to 1600 neon atoms. For these sizes, the clusters are solid and it is quite unlikely that HBr would penetrate deeply inside. Moreover, our simulations of the pick-up process also suggest that the HBr dopant stays in the surface of the cluster. We can conclude that the simulation at the $T = 0$ K within the harmonic cage approximation is not in an acceptable agreement with the photodissociation experiment of HBr picked-up on the surface of large neon clusters.

To account for finite temperature effects and for the anharmonicity of the potentials we have sampled the initial state from the semi-classical molecular dynamics simulations (see Sec. III. E). Results of such finite temperature calculations are shown in the upper part of Fig. 9 for HBr-Ne₁₃₀ and in the lower part of Fig. 9 for HBr-Ne₃₀₀. Increasing the cluster size causes only subtle changes in the resulting KED both in the experiment and in the simulations. The agreement between the simulation and the experiment is generally very good. The experimental spectrum peaks slightly steeper at the zero kinetic energy than the simulated one. This might be the result of a limited duration of the simulation. We may conclude, that both the pick-up simulations and photodissociation calculations agree now with the experiment. It is perhaps not surprising that a correct photodissociation simulation requires that the effects of temperature and anharmonicity of the floppy neon clusters has to be taken into account. If we account for anharmonicity and assume a temperature of 10 K, the neon cluster becomes larger (i.e., increased mean distance between neon atoms)

and the HBr dopant can penetrate into the surface. The HBr molecule is then no more expelled by the cluster, but it is absorbed by the liquid outer shell of the neon cluster. As a consequence, only a minor part of the photodissociating hydrogen atoms directly escapes from the cluster by reflection from the surface. We stress that even though the dopant is deeply embedded in the cluster surface, sometimes on the border line with the subsurface shell, it still has a character of the surface solvation. Namely, the asymmetry of forces still leads the librational wavefunction to be oriented towards the cluster. If the dopant occupied the subsurface substitutional position or penetrated even deeper into the cluster, the HBr would behave basically as a free rotor.

V. DISCUSSION AND CONCLUSION

The experimental results for HBr-Ne_n exhibit the same behavior in the whole measured size range from $\langle n \rangle = 100$ to 1600. The kinetic energy distributions are dominated by a peak at zero energy which indicates complete caging. The original idea to detect a transition from liquid-like to solid-like behavior in this size range, which should manifest itself in a sudden increase of the intensity at the energies of the direct cage exit caused by a rigid surface state, proved obviously to be oversimplified. In a concerted effort we tried to properly understand this experimental result theoretically. Our calculations include i) simulation of the pick-up process with the final position of the HBr molecule in the neon cluster, ii) check of the cluster phase by an instantaneous normal mode (INM) analysis, and iii) calculation of the photodissociation dynamics with the quantum preparation of the initial state at two temperatures, $T = 0$ K and the realistic $T = 10$ K. The crucial point for a realistic treatment of the neon clusters was the inclusion of the quantum character of these light clusters by a semi-classical procedure using a corrected interaction potential. The result was for the three layer system with $n = 130$ a semi-liquid core and a liquid surface and for the four layer system with $n = 300$ a solid core again with a liquid surface. In both cases, the HBr was deeply buried in this surface with the H atom pointing into the direction of the cluster. This position leads to the weak cage exit probabilities in both cases in complete agreement with the experiment. We note that this agreement is only achieved when the initial states are sampled at a finite temperature of $T = 10$ K and the quantum character of neon is accounted for.

Let us compare these results with the other information which is available for this system. There are two published quantum calculations using path integral Monte Carlo simulations. The melting temperatures are 3.5 K for Ne_7 (Ref. 57), 7.0 K for Ne_{13} , and 7.5 K for Ne_{19} (Ref. 58). These results definitely mean that these small neon clusters are liquid at 10 K, which is the experimental temperature. In an electron diffraction experiment Torchet demonstrated that larger Ne_n clusters are solid with an icosahedral structure as was found for the other heavier rare gas clusters for $\langle n \rangle = 350$ and larger clusters.⁵⁹ The transition should occur in the range $\langle n \rangle = 150$. This result is in a reasonable agreement with the present study if we take into account that this type of experiments are mainly sensitive to the volume of the cluster. Finally, two experiments were carried out in the group of Möller. In the first experiment, core level spectroscopy after the K-edge excitation in Ne_n clusters from $\langle n \rangle = 15$ to 4000 was studied using synchrotron radiation.⁶⁰ Here the characteristic peak structures were washed out up to sizes of $\langle n \rangle = 700$, again in agreement with the present findings. In the other experiment, the fluorescence excitation spectra of Xe doped neon clusters were measured.²² For the preparation by a pick-up process for $\langle n \rangle = 100$ mainly bulk states were observed. If the Xe doped neon cluster is generated in a co-expansion, again bulk states are observed for $\langle n \rangle \leq 200$ with 15-20 nearest neighbors, while bulk and surface states with 10-15 and 8-9 nearest neighbors, respectively, are present for $\langle n \rangle \geq 300$. In the pick-up preparation, the Xe goes apparently inside the cluster, in contrast to the result for HBr. This can, however, be understood by accounting for the semi-liquid behavior found in our simulation and the much deeper well depth of the Xe-Ne interaction which is with 50.1 cm^{-1} (Ref. 61) significantly larger than that for Ne-HBr (34.2 cm^{-1}). It is well known that a stronger attraction leads to a further penetration into the cluster.^{28,62} It is worth noting that also in the experiment with the co-expansion technique, where usually the minimum energy positions are reached, again the interior positions are observed up to $\langle n \rangle = 200$. For the larger clusters with a rigid core also surface positions appear, but slightly shifted inside compared to the results of the Xe doped solid argon clusters. This result is again consistent with the evidence for a liquid outer shell which we found in our simulation.

In conclusion, the photodissociation of HBr molecules prepared by the pick-up technique on Ne_n clusters differs appreciably from that for the heavier rare gases. The main experimental result is the very small cage exit probability. To explain this fact, we calculated in a concerted effort using semi-classical molecular dynamics simulations (i) the landing dur-

ing the pick-up process, (ii) the phase behavior of the cluster, and (iii) the kinetic energy distribution of the outgoing H atoms. It turned out that the outer shell was always liquid. While for the larger clusters the inner shells were solid, the smaller clusters exhibited a semi-liquid behavior. The agreement between the measured and calculated KEDs could only be obtained by accounting for the realistic finite cluster temperature of 10 K. In addition, the noticeable quantum character of the Ne_n clusters had to be taken into account. This is also the reason for the different behavior of HBr in neon vs. argon clusters.

VI. ACKNOWLEDGMENT

Support from the Czech Ministry of Education to the Center for Complex Molecular Systems and Biomolecules (Grant No. LN00A032) is gratefully acknowledged. The work in Göttingen was supported by the Deutsche Forschungsgemeinschaft in SFB 357. M.F. gratefully acknowledges the support of Alexander von Humboldt Foundation. U.B. thanks G. Torchet for sharing his unpublished results on Ne_n with us and T. Möller for helpful discussions on his data.

-
- ¹ Alimi, R.; Gerber, R. B. *Phys. Rev. Lett.* **1990**, *64*, 1453.
 - ² Schröder, T.; Schinke, R.; Liu, S.; Bačić, Z.; Moskowitz, J. W. *J. Chem. Phys.* **1995**, *103*, 9228.
 - ³ Niv, M.; Krylov, A. I.; Gerber, R. B. *Faraday Discuss. Chem. Soc.* **1997**, *108*, 243.
 - ⁴ Niv, M. Y.; Krylov, A. I.; Gerber, R. B.; Buck, U. *J. Chem. Phys.* **1999**, *110*, 11047.
 - ⁵ Žďánská, P.; Schmidt, B.; Jungwirth, P. *J. Chem. Phys.* **1999**, *110*, 6246.
 - ⁶ Schmidt, B. *Chem. Phys. Lett.* **1999**, *301*, 207.
 - ⁷ Žďánská, P.; Slavíček, P.; Jungwirth, P. *J. Chem. Phys.* **2000**, *112*, 10761.
 - ⁸ Baumfalk, R.; Nahler, N. H.; Buck, U.; Niv, M. Y.; Gerber, R. B. *J. Chem. Phys.* **2000**, *113*, 329.
 - ⁹ Slavíček, P.; Žďánská, P.; Jungwirth, P.; Baumfalk, R.; Buck, U. *J. Phys. Chem.* **2000**, *104*, 7793.
 - ¹⁰ Slavíček, P.; Roeselová, M.; Jungwirth, P.; Schmidt, B. *J. Chem. Phys.* **2001**, *114*, 1539.
 - ¹¹ Monnerville, M.; Pouilly, B. *Chem. Phys. Lett.* **1998**, *294*, 473–479.

- ¹² Trin, J.; Monnerville, M.; Pouilly, B.; Meyer, H. D. *J. Chem. Phys.* **2003**, *118*, 600–609.
- ¹³ Lepetit, B.; Lemoine, D. *J. Chem. Phys.* **2002**, *117*, 8676–8685.
- ¹⁴ Prosmitti, R.; García-Vela, A. *J. Chem. Phys.* **2002**, *117*, 100–109.
- ¹⁵ García-Vela, A. *J. Chem. Phys.* **1998**, *108*, 5755.
- ¹⁶ Narevicius, E.; Moiseyev, N. *Chem. Phys. Lett.* **1998**, *287*, 250–254.
- ¹⁷ Baumfalk, R.; Buck, U.; Frischkorn, C.; Gandhi, S. R.; Lauenstein, C. *Ber. Bunsenges. Phys. Chem.* **1997**, *101*, 606.
- ¹⁸ Baumfalk, R.; Nahler, N. H.; Buck, U. *Faraday Discuss.* **2001**, *118*, 247.
- ¹⁹ Buck, U. *J. Phys. Chem. A* **2002**, *106*, 10049.
- ²⁰ Kreher, C.; Carter, R.; Huber, J. R. *J. Chem. Phys.* **1999**, *110*, 3309.
- ²¹ Li, Q.; Huber, J. R. *Chem. Phys. Lett.* **2001**, *345*, 415.
- ²² von Pietrowski, R.; Rutzen, M.; von Haefen, K.; Kakar, S.; Möller, T. *Z. Phys. D* **1997**, *40*, 22.
- ²³ Schmidt, M.; Kusche, R.; von Issendorff, B.; Haberland, H. *Nature* **1998**, *393*, 238.
- ²⁴ Rytönen, A.; Valkealahti, S.; Manninen, M. *J. Chem. Phys.* **1997**, *106*, 1888–1892.
- ²⁵ Ehrenfest, P. *Z. Physik* **1927**, *45*, 455.
- ²⁶ Buck, U.; Galonska, R.; Kim, H. J.; Lohbrandt, P.; Lauenstein, C.; Schmidt, M. In *Atomic and Molecular Beams. The State of the Art 2000*; Campargue, R., Ed.; Springer: Berlin, 2001; page 623.
- ²⁷ Baumfalk, R.; Buck, U.; Frischkorn, C.; Nahler, N. H.; Hüwel, L. *J. Chem. Phys.* **1999**, *111*, 2595.
- ²⁸ Nahler, N. H.; Baumfalk, R.; Buck, U.; Vach, H.; Slavíček, P.; Jungwirth, P. *Phys. Chem. Chem. Phys.* **2003**, *XX*, xxx.
- ²⁹ Hagena, O. F. *Surf. Sci.* **1981**, *106*, 101.
- ³⁰ Aziz, R. A.; Slaman, M. J. *J. Chem. Phys.* **1989**, *130*, 187–194.
- ³¹ Herzberg, G. *Molecular Spectra and Molecular Structure*; Van Nostrand: New York, 1950.
- ³² Peoux, G.; Monnerville, M.; Duhoo, T.; Pouilly, B. *J. Chem. Phys.* **1997**, *107*, 70.
- ³³ Miguel, B.; Bastida, A.; Zuñiga, J.; Requena, A.; Halberstadt, N. *J. Chem. Phys.* **2000**, *113*, 10130–10142.
- ³⁴ Schiff, L. I. *Quantum Mechanics, 3rd ed.*; McGraw-Hill: New York, 1968.
- ³⁵ Sterling, M.; Li, Z.; Apkarian, V. A. *J. Chem. Phys.* **1995**, *103*, 5679.

- ³⁶ Feynman, R. P.; Hibbs, A. R. *Quantum Mechanics and Path Integrals*; McGraw Hill: New York, 1965.
- ³⁷ Sesé, L. M. *Mol. Phys.* **1993**, *78*, 1167.
- ³⁸ Portwich, G. Semiklassische Simulation von Stoßprozessen zwischen Fremdatomen und großen Heliumclustern Master's thesis, Universität Göttingen, **1995**.
- ³⁹ Vach, H. *J. Chem. Phys.* **2000**, *113*(3), 1097–1103.
- ⁴⁰ Allen, M. P.; Tildesley, D. J. *Computer Simulations of Liquids*; Clarendon Press, Oxford, 1987.
- ⁴¹ Schütte, S.; Buck, U. *Intern J. Mass Spectr.* **2002**, *220*, 183.
- ⁴² Keyes, T. *J. Phys. Chem. A* **1997**, *101*, 2921–2930.
- ⁴³ Stratt, R. M. *Accounts Chem. Res* **1995**, *28*, 201–207.
- ⁴⁴ Adams, J. E.; Stratt, R. M. *J. Chem. Phys.* **1990**, *93*, 1332–1346.
- ⁴⁵ Adams, J. E.; Stratt, R. M. *J. Chem. Phys.* **1990**, *93*, 1632–1640.
- ⁴⁶ Buch, V. *J. Chem. Phys.* **1990**, *93*, 2631–2639.
- ⁴⁷ Chakravarty, C.; Ramaswamy, R. *J. Chem. Phys.* **1997**, *106*, 5564–5568.
- ⁴⁸ Hillery, M.; O'Connell, R. F.; Scully, M. O.; Wigner, E. P. *Phys. Rep.* **1984**, *106*, 121–167.
- ⁴⁹ Slavíček, P.; Jungwirth, P.; Lewerenz, M.; Nahler, N. H.; Fárnik, M.; Buck, U. *J. Chem. Phys.* **2003**, *xxx*, xxxx.
- ⁵⁰ Nahler, N. H.; Fárnik, M.; Buck, U.; Vach, H.; Niv, M.; Gerber, R. B. *J. Chem. Phys.* **2003**, page in preparation.
- ⁵¹ Buck, U. *Surf. Rev. Lett.* **1996**, *3*, 467.
- ⁵² Schröder, T.; Schinke, R.; Krohne, R.; Buck, U. *J. Chem. Phys.* **1997**, *106*, 9067.
- ⁵³ Farges, J.; de Feraudy, M. F.; Raoult, B.; Torchet, G. *Sur. Sci.* **1981**, *106*, 95.
- ⁵⁴ Dickey, J. M.; Paskin, A. *Phys. Rev.* **1969**, *188*, 1407–1418.
- ⁵⁵ Leake, J. A.; Daniels, W. B.; J. Skalyo, J.; Frazer, B. C.; Shirane, G. *Phys. Rev.* **1969**, *181*, 1251–1260.
- ⁵⁶ Bilz, H.; Kress, W. *Phonon Dispersion Relations in Insulators*; Springer, Berlin, 1979.
- ⁵⁷ Beck, T. L.; Doll, J. D.; Freeman, D. L. *J. Chem. Phys.* **1989**, *90*, 5651.
- ⁵⁸ Chakravarty, C. *J. Chem. Phys.* **1995**, *102*, 956–962.
- ⁵⁹ private communication. Torchet, G.
- ⁶⁰ Kakar, S.; Björneholm, O.; Löffken, J. O.; Federmann, F.; Soldatov, A. V.; Möller, T. *Z. Phys. D* **1997**, *40*, 84.

⁶¹ Aziz, R. In *Inert Gases*; Klein, M. L., Ed.; Springer, Berlin, 1984; page 5.

⁶² Vach, H. *J. Chem. Phys.* **1999**, *111*, 3536.

	HBr—Ne _n					HCl—Ne _n		
diameter of conical nozzle / μm	47	40	40	40	40	40	40	40
nozzle opening angle α / degrees	30°	20°	20°	20°	20°	20°	20°	20°
expansion pressure / bar	8.5	8.0	8.0	8.0	8.0	8.0	8.0	8.0
nozzle temperature / K	107	105	94	87	61	114	105	72
average cluster size $\langle n \rangle$	143	200	300	400	1600	147	200	800
pick-up pressure / 10^{-2} mbar	2	4	4	4	4	4	4	4

TABLE I: Beam data of the Ne clusters

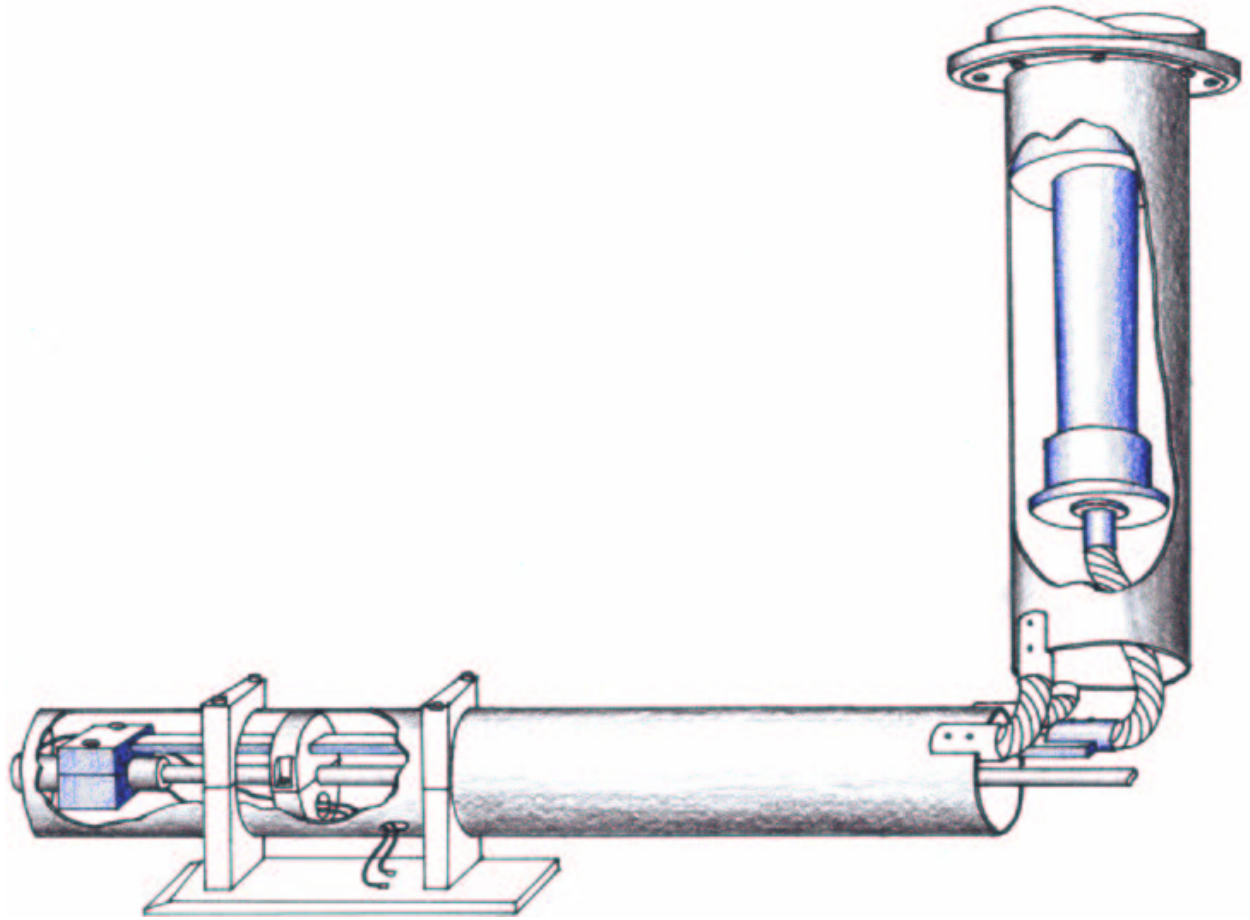


FIG. 1: Source for the generation of big Ne clusters. Horizontal plane: the nozzle on the very left mounted to a stainless steel pipe for the Ne gas (coming from the right) and surrounded by a copper block connected to the second stage of the He cryo-pump (vertical in the middle). The whole assembly is shielded by a copper tube. The shield is connected to the first stage of the cryo pump to avoid thermal radiation onto the source. Vertical plane: He cryo pump with copper tubes mounted. The vertical and horizontal copper parts are connected with copper cables of 10 mm diameter.

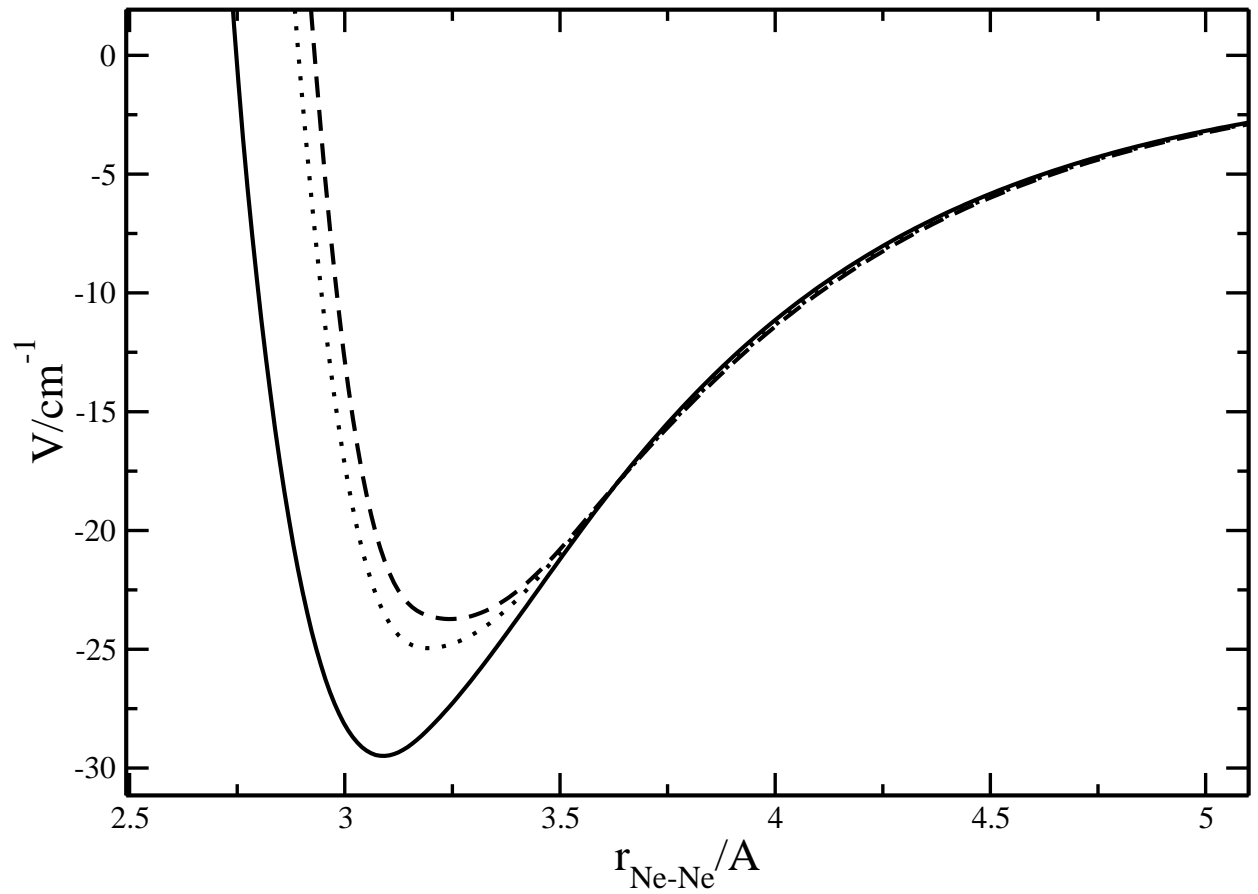


FIG. 2: Convergence of effective Ne-Ne potential at $T = 10$ K. The full line is the classical potential, the dashed line the first iteration step and the long dashed line is the converged potential corrected for quantum effects.

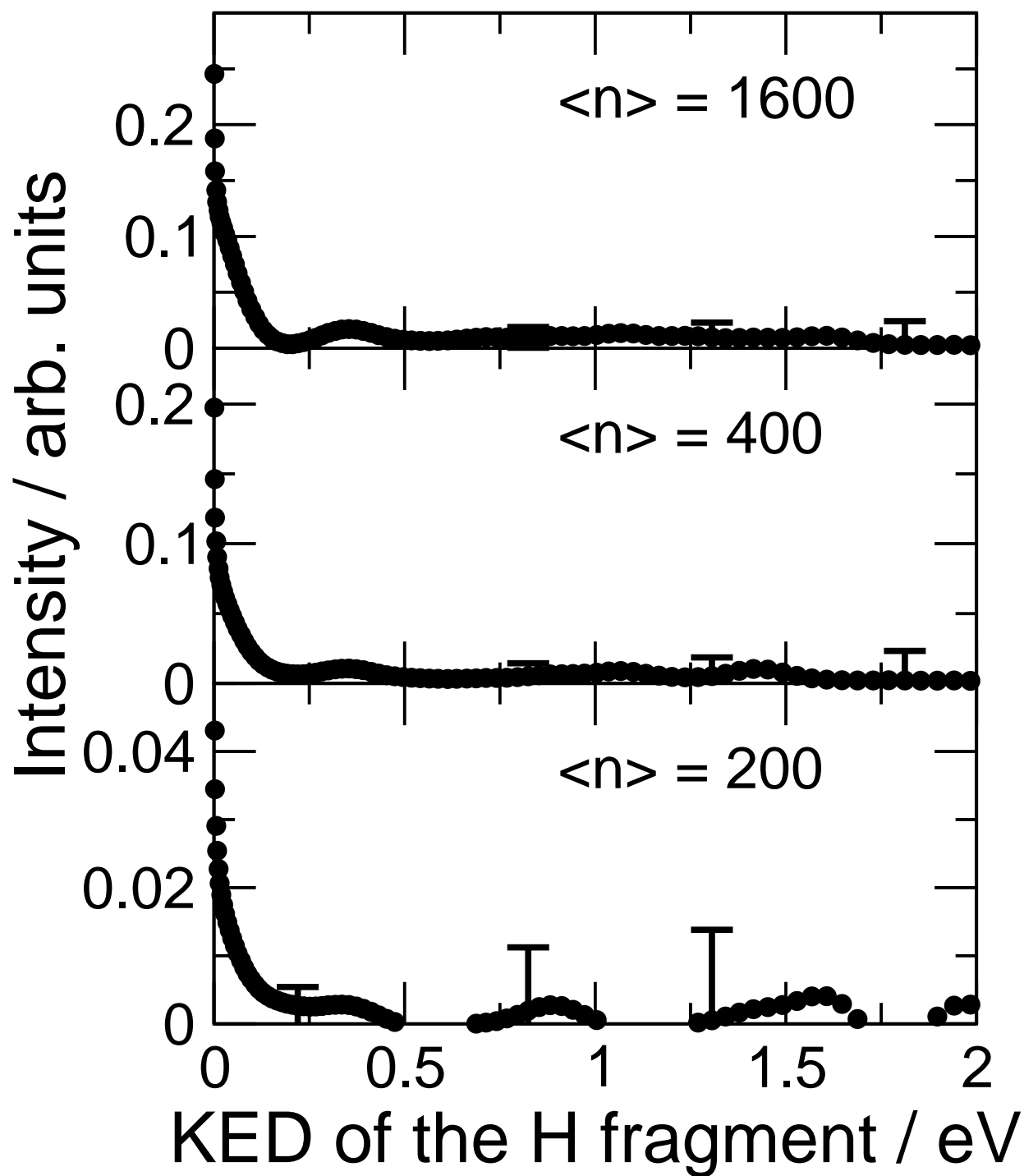


FIG. 3: Measured kinetic energy distributions for HBr—Ne_n with different average cluster sizes prepared in a pick-up process.

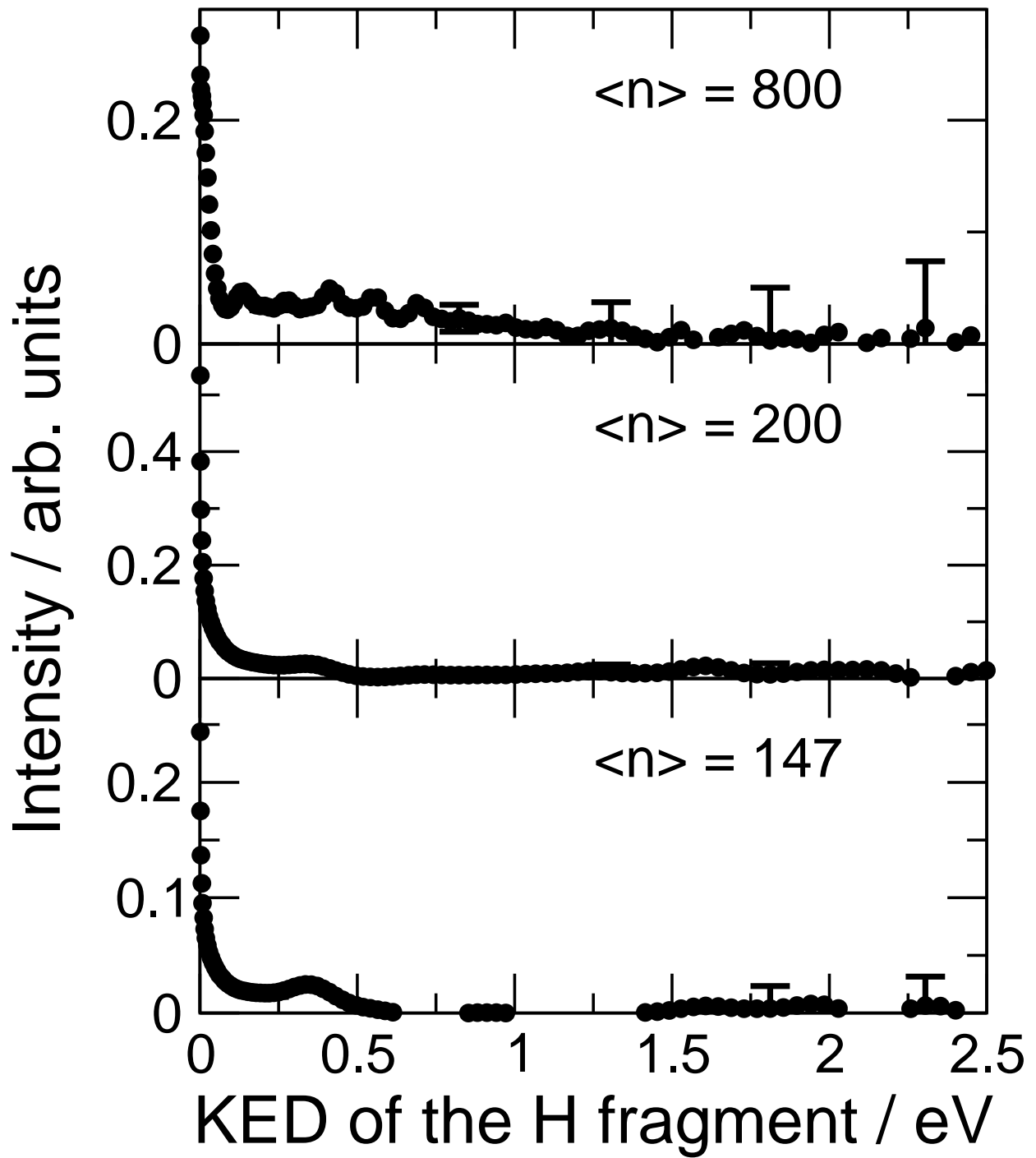


FIG. 4: Measured kinetic energy distributions of HCl-Ne_n for different average cluster sizes prepared in a pick-up process.

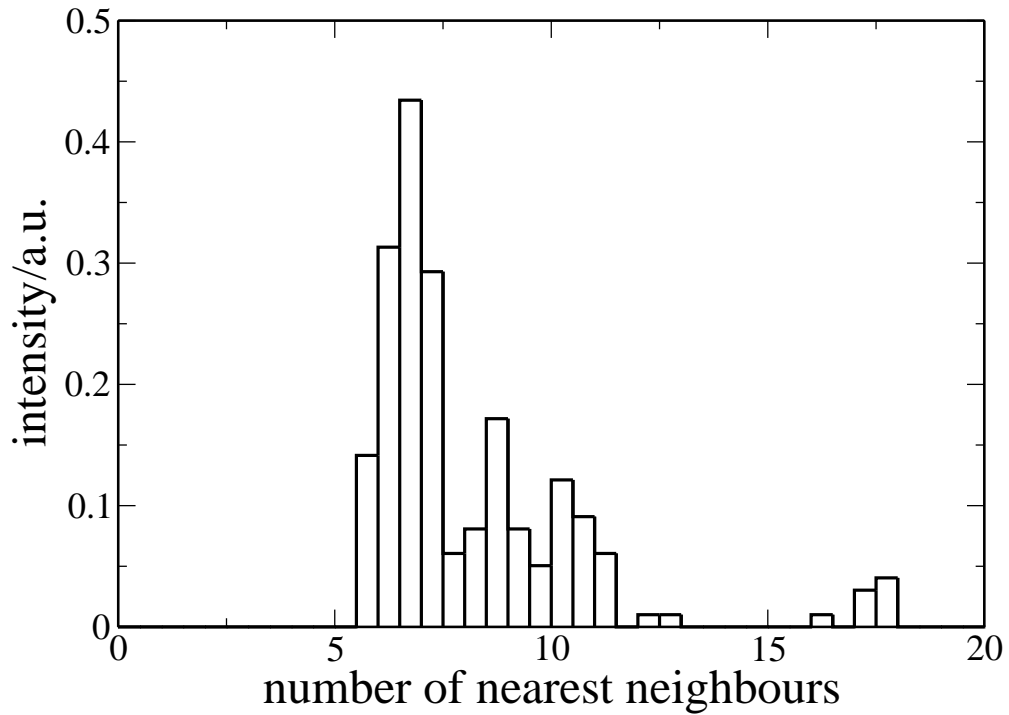
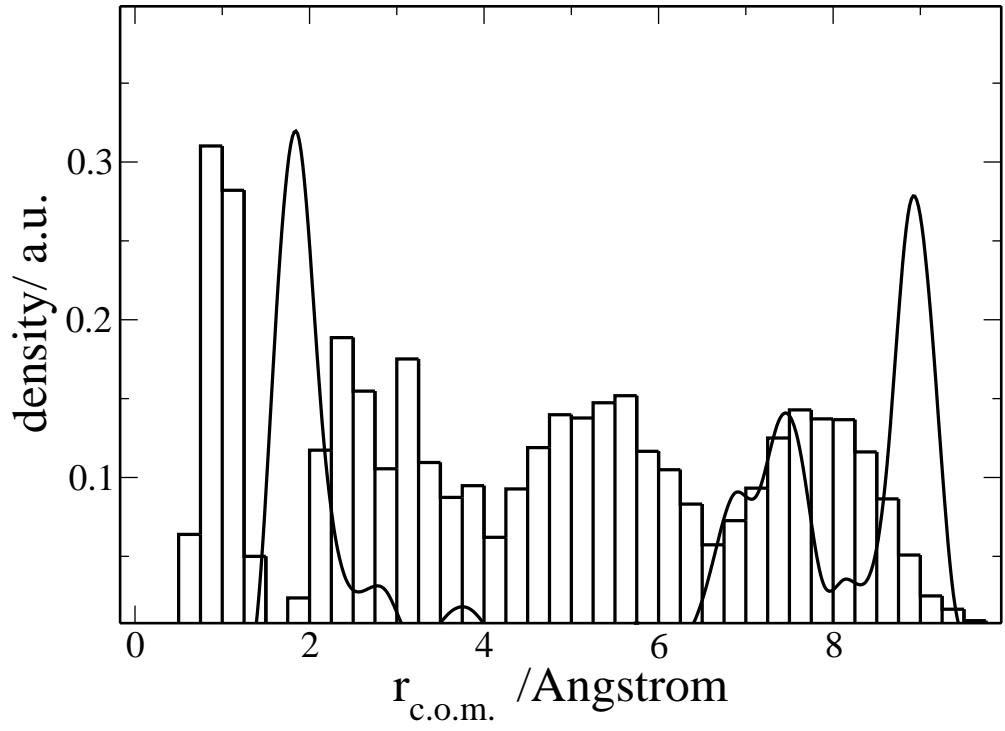


FIG. 5: Pick-up of HBr on a Ne_{130} cluster. Upper panel: Density of dopant atoms (solid line) in comparison with the density of neon atoms (histogram). Densities are for convenience scaled. Lower panel: Distribution of the number of nearest neighbors of the dopant atom.

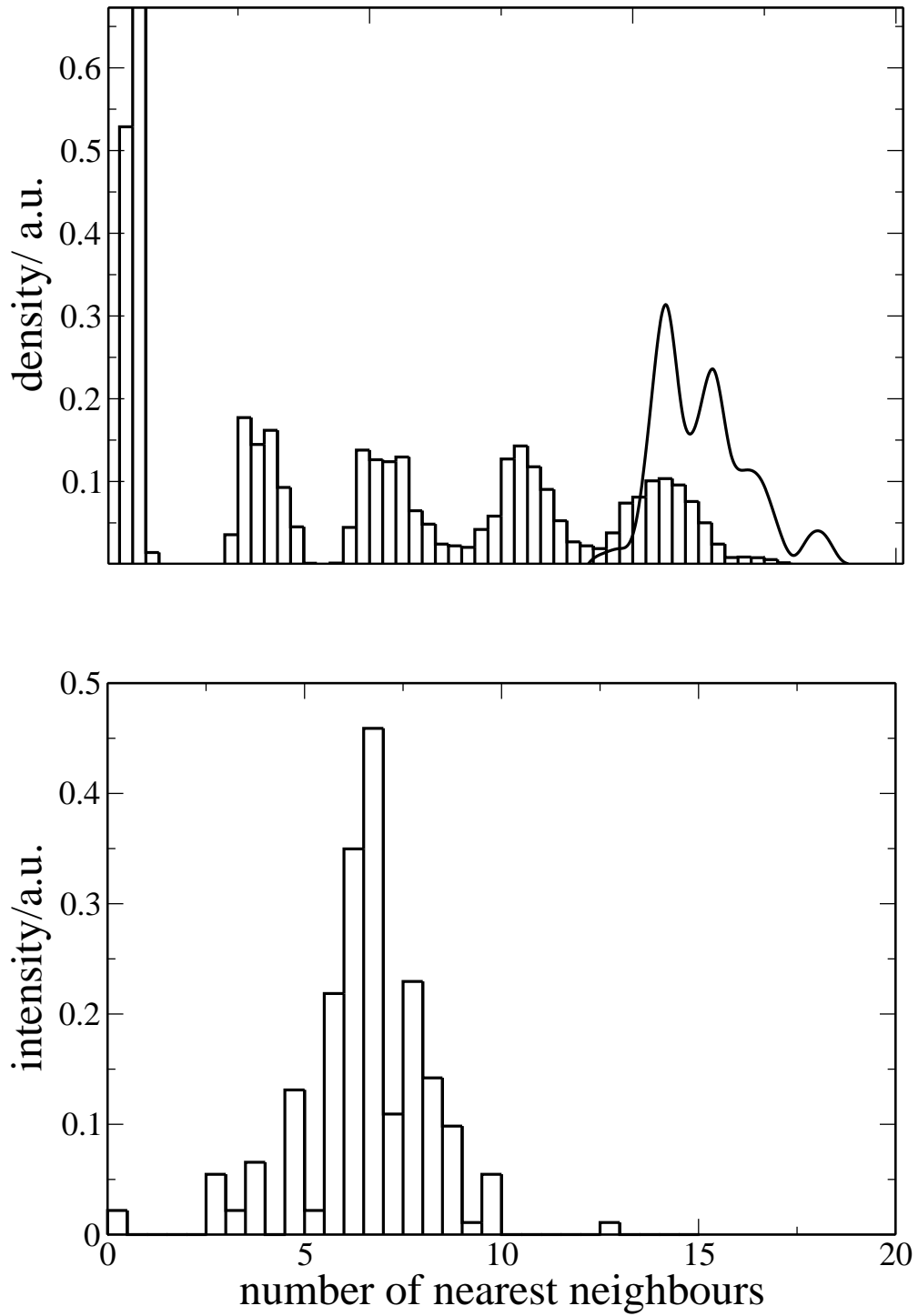


FIG. 6: Pick-up of HBr on a Ne_{300} cluster. Upper panel: Density of dopant atoms (solid line) in comparison with the density of neon atoms (histogram). Densities are for convenience scaled. Lower panel: Distribution of the number of nearest neighbors of the dopant atom.

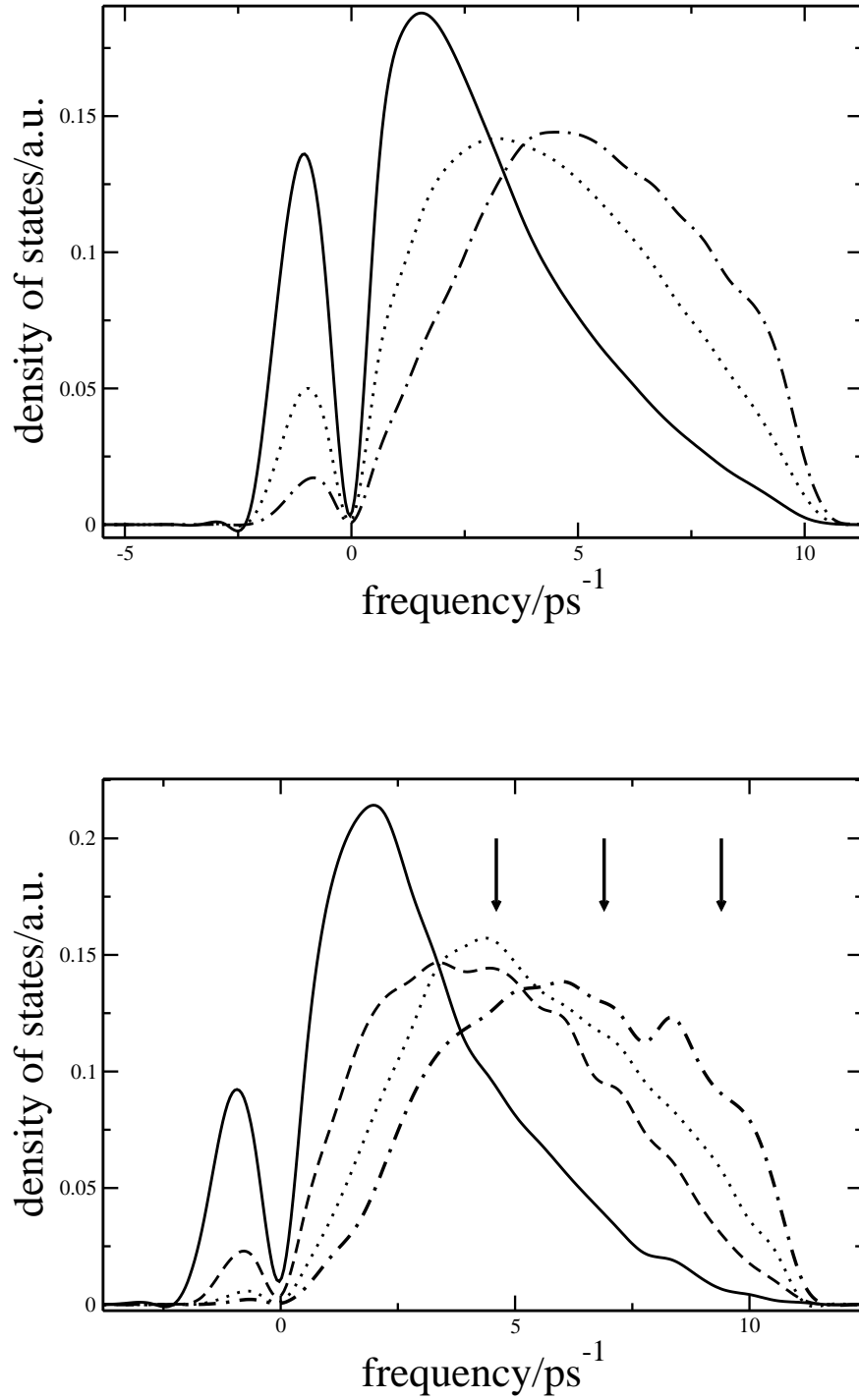


FIG. 7: INM density of states of different layers in neon clusters. All density distributions are normalized. Imaginary frequencies are displayed on the negative axis. Upper panel: Ne_{130} cluster. Outer shell-solid line, medium layer-dotted line, inner part of the cluster-dashed-dotted line. Lower panel: Ne_{300} cluster. Outer shell-solid line, third shell-dashed line, second layer-dotted line, inner part of the cluster-dashed-dotted line. The arrows indicate the positions of the transverse and longitudinal peaks of the phonon spectrum of solid neon.⁵⁶

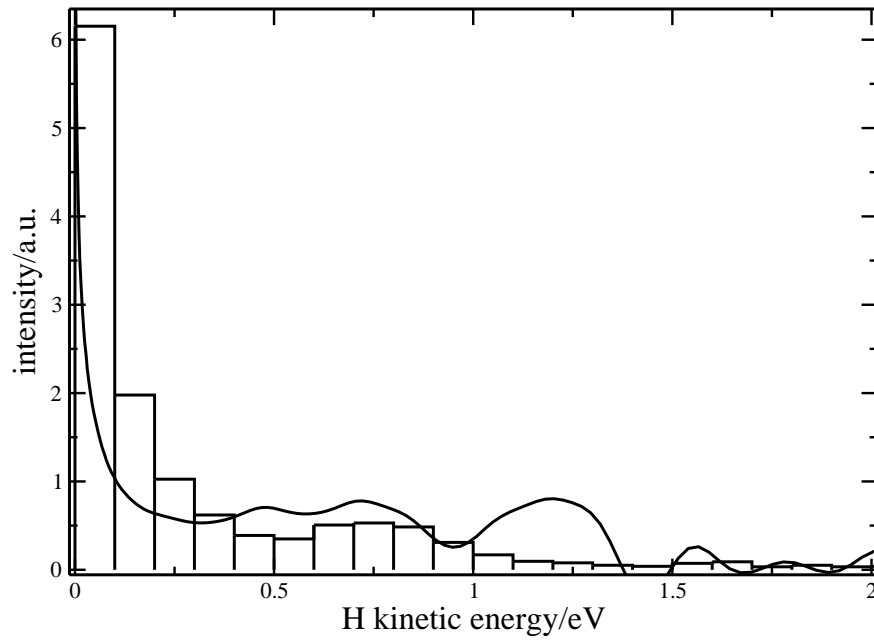
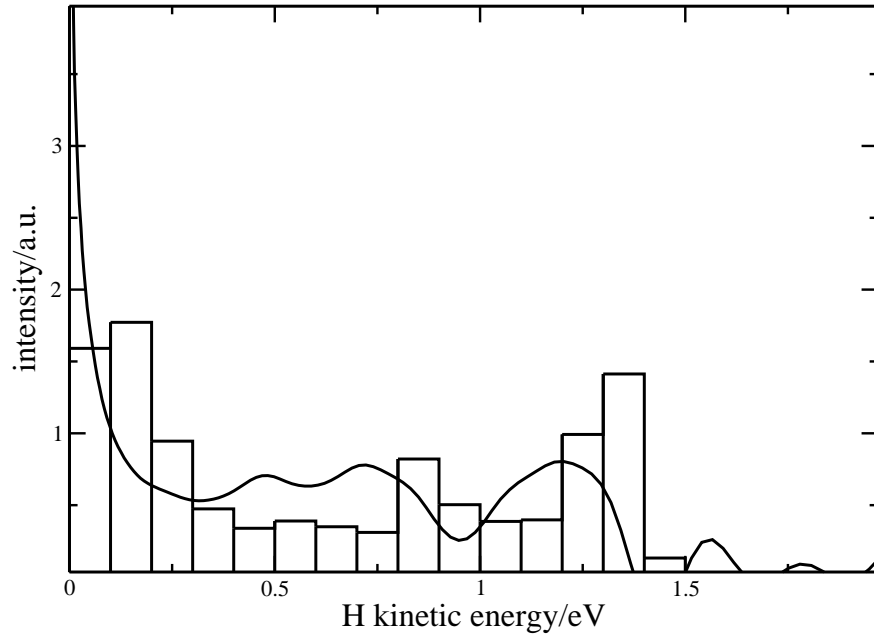


FIG. 8: Photodissociation of the HBr-Ne $_n$ cluster. The points represent experimental result for clusters prepared by the pick-up procedure for the average size $\langle n \rangle = 143$. The histograms display results of the simulation of HBr-Ne $_{146}$ at $T = 0$ K; upper panel: HBr on the surface of the cluster; lower panel: HBr embedded in the center of the cluster.

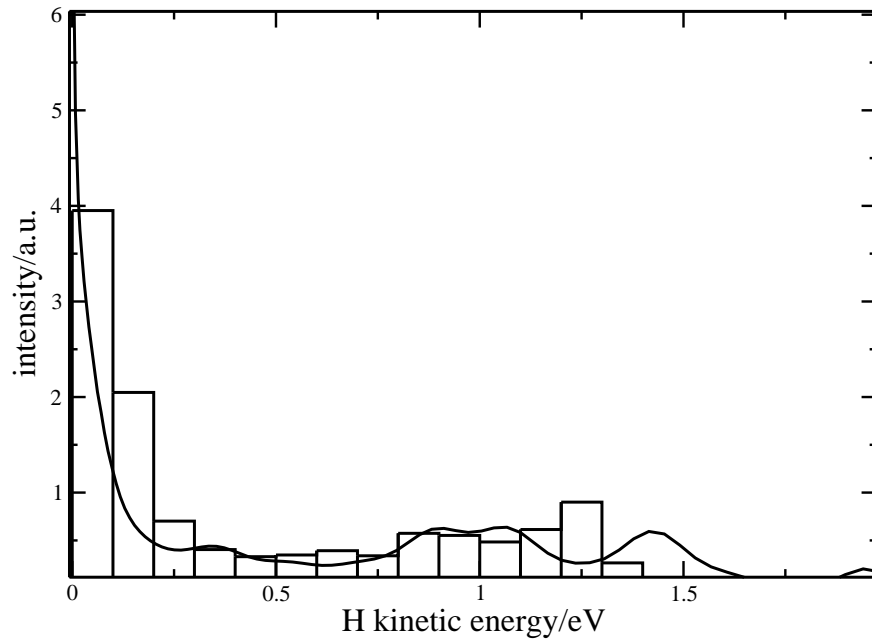
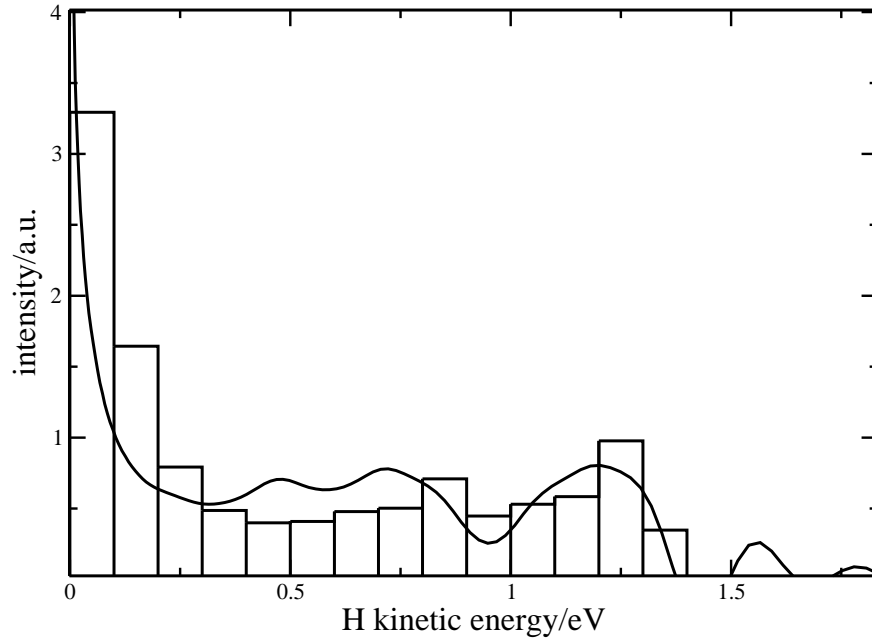


FIG. 9: Photodissociation of HBr-Ne $_n$ clusters. The points represent experimental result for clusters prepared by the pick-up procedure. Upper panel: $\langle n \rangle = 143$. The histograms display results of the simulation of HBr-Ne $_{\approx 130}$ at $T = 10$ K. Lower panel: experiments for $\langle n \rangle = 300$ and simulations for HBr-Ne $_{\approx 300}$ at $T = 10$ K.